CHEMISTRY
A EUROPEAN JOURNAL

DOI: 10.1002/chem.200800544

Well-Controlled Synthesis of Au@Pt Nanostructures by Gold-Nanorod-Seeded Growth

Lili Feng,[a, c] Xiaochun Wu,*[a] Lirong Ren,[a] Yanjuan Xiang,[b] Weiwei He,[a, c] Ke Zhang,[a, c] Weiya Zhou,[b] and Sishen Xie*[b]

Abstract: Pt nanodots were formed on Au nanorods (NRs) by using a simple seed-mediated growth. Their density and distribution on the Au NR can be finely tuned by varying the reaction parameters. At lower Pt/Au ratios, the Pt nanodots mainly appear at endcaps and side edges of the Au rod. At higher Pt/Au ratios, they distribute homogeneously over the whole Au rod. The obtained Pt nanostructure is a single crystal owing to the epitaxial growth of Pt on the Au rod. Due to the unique surface plasmon resonance (SPR) features of the Au NRs, the Au core/Pt shell (Au@Pt) nanostructures also exhibit well-defined and red-shifted longitudinal SPR bands in the visible and near-infrared region. The position and intensity can be regulated by the thickness and amount of the Pt shell. At a thinner Pt thickness, the Au@Pt NRs show higher dielectric sensitivity than the corresponding Au NRs. It thus opens up the potential of Pt nanostructures for SPR-based sensing.

Keywords: crystal growth · gold · nanostructures · platinum · surface plasmon resonance

Introduction

Nanostructured platinum plays an important role in many industrial applications, with the catalytic properties of Pt especially emphasized. For example, platinum can catalyze the reduction of pollutant exhaust gases from automobiles. These catalytic properties are closely related to its dimension, morphology, and structures.[1] Therefore, much effort has been devoted to the synthesis of Pt nanostructures with controlled sizes and well-defined morphology and structure.[2] Among such structures, porous nanoscale structures are especially desirable due to the enlarged surface area.[3] Apart from monometallic Pt, bimetallic nanostructures have also attracted a great deal of attention due to their improved properties over the monometallic counterpart for special cases.[4] For example, for CO-contaminated H_2 fuels at low-temperature, CO-tolerant H_2 electrocatalysts are desired. Au nanoparticles can effectively catalyze the CO oxidation, but they are ineffective as the electrocatalysts for H_2 oxidation. In contrast, Pt nanoparticles, albeit efficient for H_2 activators, are poisoned by CO below 100 °C. Zhou et al. synthesized an Au/Pt heteroaggregate with an 11 nm Au core and 5 nm of dendritic Pt on the Au surface.[5] The Au/Pt heteroaggregate catalysts showed a remarkable enhancement in CO tolerance (1000 ppm), while maintaining their catalytic activity. Both the bimetallic nature and heteroaggregate architecture were believed to play a key role. In another case, Zhao et al. demonstrated a Au/Pt core-shell nanostructure with an improved Pt utilization of nearly 100% for methanol electro-oxidation.[6]

In contrast to the catalytic properties, the surface plasmon resonance (SPR) properties of Pt and Pd nanoparticles remain largely unexplored, because their SPR bands (with particle sizes less than 10 nm) are located in the UV region. Recently, by tailoring the shape and structure of Pd and Pt nanoparticles, their SPR bands have been pushed to the visible region. For example, Xia's group has synthesized palladium triangles, hexagons, and cubes of several nanometers. By tailoring the shape of Pd nanoparticles to triangular and hexagonal nanoplates, their SPR bands can be pushed into the visible region (520 nm).[7a] In addition, they further dem-

[a] L. Feng, Prof. Dr. X. Wu, Dr. L. Ren, W. He, K. Zhang
National Center for Nanoscience and Technology
Zhongguancun, Beiyitiao No. 11, Beijing, 100190 (P. R. China)
Fax: (+86) 10-8254-5577
E-mail: wuxc@nanoctr.cn

[b] Dr. Y. Xiang, Prof. Dr. W. Zhou, Prof. Dr. S. Xie
National Laboratory for Condensed Matter Physics
Institute of Physics, Beijing, 100080 (P. R. China)
Fax: (+86) 10-82640215
E-mail: ssxie@aphy.iphy.ac.cn

[c] L. Feng, W. He, K. Zhang
Graduate School of the Chinese Academy of Sciences
Beijing, 100080 (P. R. China)

WILEY InterScience DISCOVER SOMETHING GREAT
© 2008 Wiley-VCH Verlag GmbH & Co. KGaA, Weinheim

onstrated that the formation of hollow structures could also push the SPR band into the visible region. In the case of Pd nanoparticles with the same size of 48 nm, simply changing the structure allows the SPR band to be tuned from 410 nm for nanocubes, to 450 nm for nanoboxes, and further to 520 nm for nanocages with a wall thickness of 6 nm.[7b] This makes the use of their SPR characteristics possible. Due to the improved SPR properties, their applications in surface enhanced Raman scattering (SERS) have also been explored.[7] Apart from tuning the size and shape of Pt and Pd nanoparticles, another way to improve their optical properties is the formation of the bimetallic structure.[8] Traditionally, Au and Ag nanoparticles exhibit strong and sharp SPR features and high SERS activities. By forming core/shell structures with Au or Ag, the optical properties of Pt and Pd can be improved. For instance, by assembling Au/Pt core/shell (Au@Pt) nanoparticles on a glass carbon anode surface, Zhang et al. found good SERS signals for CO and thiocyanate (SCN^-) absorbed on the anode.[8b] With respect to depositing a Pt film directly on a coarse Au anode, one advantage of Au@Pt nanoparticles is that the SERS activities can be adjusted by changing the shell structure and thickness.

Considering the improved properties of bimetallic nanoparticles over monometallic ones, controlled syntheses with desired size and structure become important. A variety of methods has been developed to prepare Au@Pt nanoparticles.[9] For example, Au/Pt bimetallic nanoflowers have been fabricated on a polyamidoamine dendrimer-modified surface through electrodeposition.[10] Recently, high-quality single-crystalline gold nanorods (NRs) have been synthesized by seed-mediated growth.[11] The greatly enhanced SPR features and SPR positions that are easily tunable by simply changing the aspect ratios (length versus width) make them attractive for SPR and SERS-based sensing.[12] Herein, using Au NRs as seeds, we report a simple method for the preparation of Au@Pt nanostructures under mild conditions. Pt nanodots were formed on the Au nanorod, and their density and distribution could be finely controlled, with both edge growth and homogeneous growth realized. Importantly, due to the unique SPR features of the Au core, the Au@Pt nanostructures exhibit well-defined and red-shifted longitudinal SPR (LSPR) bands in the visible and near-infrared region. The origin of these bands can be considered as the combination of the Au core and the Pt shell. With a fixed Au core, the LSPR features of Au@Pt nanostructures can be regulated by the thickness of the Pt shell. At a thinner Pt thickness, the LSPR band of the Au core still dominates, albeit damped and broadened a little by the Pt shell. A well-defined LSPR band in the visible and near-infrared region makes the exploration of its dielectric sensitivity possible. At a thinner Pt thickness, the red-shifted and slightly broadened LSPR band exhibits an even higher dielectric sensitivity than the LSPR band of the corresponding Au core. This therefore opens up the potential of using Pt nanostructures for SPR-based sensing.

Results and Discussion

The morphology and SPR features of the Au@Pt nanostructures: Figure 1a is a typical SEM image of the gold nanorods obtained through seed-mediated growth. The Au NR has a cylindrical shape with eight side surfaces. Often, three edges are observed. The average aspect ratio of the Au NRs here is 3.5. The deposition of Pt on the Au NR can be divided into three cases according to the molar ratio of Pt/Au. At Pt/Au ratios less than 0.2 (case 1), small Pt nanodots are observed mainly at the endcaps and edges of the Au rod, thus making the edges more evident (Figure 1b and c). At Pt/Au ratios larger than 0.2 (case 2), small Pt nanodots also appear

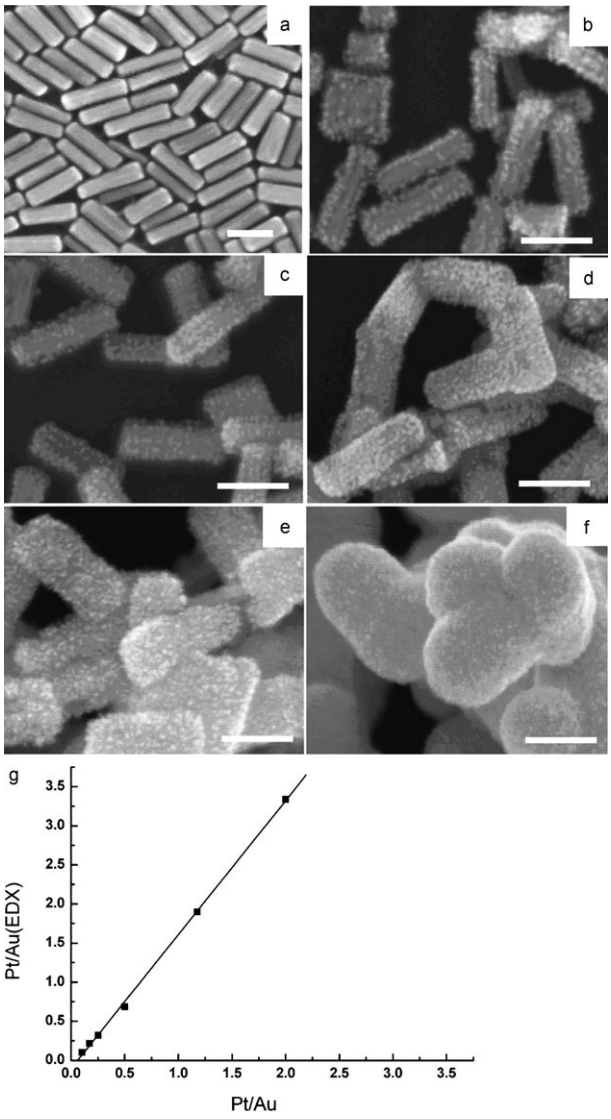

Figure 1. SEM images of a) the Au NRs, and b)–f) the Au@Pt nanostructures with calculated Pt/Au ratios of b) 0.17, c) 0.25, d) 0.5, e) 1.17, and f) 2. The scale bar is 50 nm, and the AA/Pt ratio is 10. g) The relationship between the calculated Pt/Au molar ratios and those measured by EDX analysis.

 © 2008 Wiley-VCH Verlag GmbH & Co. KGaA, Weinheim

on the flat side surfaces; thus the Pt nanodots cover the Au rod homogeneously (Figure 1d and e). The density of Pt nanodots increases with increasing Pt/Au ratios (from 0.2 to 1.2). The overall aspect ratio decreases with an increasing amount of Pt. At the Pt/Au ratio of 0.5, instead of separate nanorods, end-to-end connected nanorods often appear. At the Pt/Au ratio of 2 (case 3), much larger Pt nanostructures form (Figure 1f). By checking the broken Pt nanostructures, it is found that several gold nanorods are involved in the formation of one Pt nanostructure, and the original shape of the Au NR is not easily distinguishable. Additionally, aggregates are the dominant morphologies.

Energy-dispersive X-ray (EDX) analysis verified the deposition of Pt. The actual Pt/Au molar ratios (averaged from five consecutive measurements) by EDX show a good linear relationship with the calculated ones, indicating that a determined amount of ionic Pt is transformed into Pt atoms.

Figure 2 shows the UV/Vis/NIR absorption spectra of the as-prepared Au NRs and Pt-coated Au NRs. According to the calculated amount of Pt deposited on the Au NRs, we

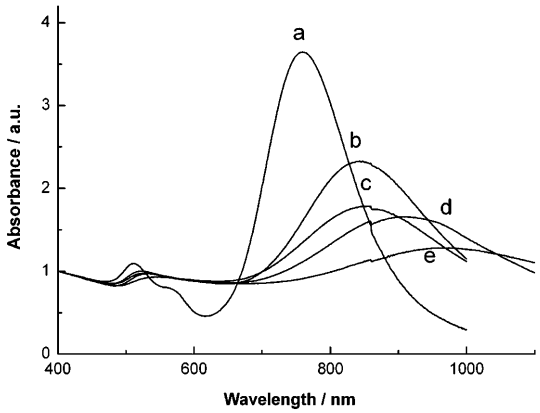

Figure 2. UV/Vis/NIR absorption spectra of a) the Au NRs, and b–e) the Au@Pt nanostructures. The calculated Pt/Au molar ratios were b) 0.1, c) 0.17, d) 0.25, and e) 0.5.

named the obtained nanorods as Au@Pt*n*, in which *n* denotes the molar ratio of Pt/Au within the Au@Pt nanorod. To compare the effect of the Pt amount on the SPR features of the Au NRs, each spectrum was normalized by its absorption at 400 nm. The as-prepared Au NRs show a strong LSPR band centered at 760 nm, with a full width at half maximum (FWHM) value of 0.33 eV and a weak transverse SPR band around 512 nm. By depositing Pt on the nanorods the LSPR band is gradually red-shifted, accompanied by a great reduction in intensity and an evident broadening in width. From Au@Pt0.1 to Au@Pt0.25 (Figure 2b–d), the Pt-coated gold NRs remain as separate entities. The increased reduction and broadening of the LSPR band are due to the enhanced damping of Pt. Interestingly, although the overall aspect ratio is decreasing, the LSPR band is red-shifted. For Au@Pt0.5 (Figure 2e) the changes in the LSPR features are more complex, due to the contribution of coupling between the connected Pt nanostructures, and will not be discussed here. For Au@Pt1.17 and Au@Pt2, due to the severe aggregation of the Pt nanostructures, we could not obtain the proper UV/Vis absorption spectra.

Using Au NRs as templates, Au@Pt and Au@Pd nanorods with homogeneously coated Pt or Pd nanodots have been reported.[13,14] The structure of the Pt shell, however, has not been investigated. In the case of Au@Pd nanorods, Pd nanodots with a polycrystalline structure were suggested.[14] The large lattice mismatch between Pd (0.389 nm) and Au (0.408 nm) was believed to induce the random nucleation of the Pd nanodots, thus a polycrystalline structure. To gain more insight into the structure of the Pt shell, high-resolution TEM (HRTEM) images were measured. In Figure 3A–C, one sample with Pt nanodots grown at two endcaps and edges of the Au NR was employed. The SEM image verified the locations of these Pt nanodots (Figure 3A). From the HRTEM image, we can see that the Pt shell is a single crystalline structure. The lattice plane distance is 0.196 nm, corresponding to a lattice plane distance of Pt {002}. This is also confirmed by the corresponding fast Fourier transform (FFT) analysis (in the inset): the FFT pattern corresponds to only one set of diffraction spots: {002}. This means that instead of random nucleation, there exists an epitaxial Pt layer on the surface of the Au NR. Small Pt nanodots with sizes of 3–4 nm are epitaxial protrusions of the Pt shell on the endcaps and edges of the Au NR. In Figure 3D–F, an Au@Pt nanostructure with Pt nanodots grown homogeneously over the whole surface of the Au NR was checked. In the SEM image, the Pt nanostructure covers the Au NR homogeneously. In the low-magnification TEM image, the Au core and Pt shell can be distinguished clearly. The obtained Pt shell is thicker and more compact than that of Figure 3C. The HRTEM image verified that the Pt shell is still single crystalline in nature. In Figure 3F, the {002} lattice planes of Pt are imaged, indicating that the electron beam is aligned in the [001] direction. In addition, apart from the {002}, in the FFT, high lattice indices were also observed. They are different from the low lattice indices, indicating the appearance of nanodots with different orientations at higher Pt/Au ratios. Based on these observations, we suggest the following growth mode: an epitaxial Pt layer first formed on the surface of the Au NR. At lower Pt/Au ratios, epitaxial protrusions preferentially formed at edges and endcaps, possibly due to more structural defects and fewer orderly packed CTAB molecules at these locations. At higher Pt/Au ratios, due to a large number of available Pt ions for each Au NR, the preferential edge-growth conditions were destroyed. Pt protrusions formed both at edges and on the flat surfaces. Recently, spherical Pt nanodendrites have been made with a single-crystalline structure, for which a seeding/autocatalytic growth mechanism was suggested.[15] The same growth mechanism, we believe, also works here. Recently, by coating Pd on the Au NR, we synthesized rectangular Au@Pd nanobars with a single-crystalline structure.[16] The lattice mismatch between Pt and Au (3.8%) is smaller than that between Pd and Au (4.7%). Therefore, the lattice mismatch

 © 2008 Wiley-VCH Verlag GmbH & Co. KGaA, Weinheim

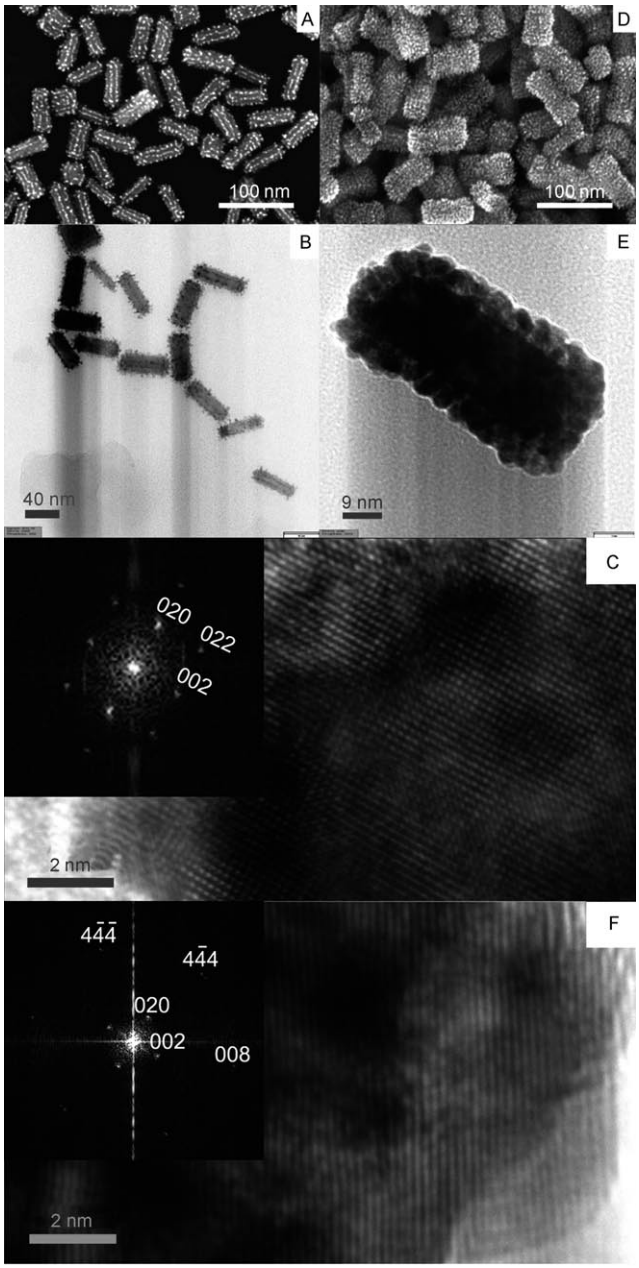

Figure 3. SEM and TEM images of the Au@Pt nanostructures with Pt nanodots coated at edges (A, B, and C) and on the whole surface (D, E, and F) of the Au NR. The electron beam was aligned along the [001] direction for C and F.

is not a critical factor in determining the morphologies of the Au@Pt nanorods and the rectangular Au@Pd nanobars. Further investigation is needed to understand the different growth behaviors of Pt and Pd on the Au NR.

Tuning the LSPR positions of the Au@Pt nanorods by varying Pt thickness: As shown in Figure 2, at Pt/Au ratios lower than 0.25, the LSPR band of the Au@Pt nanorods is red-shifted with decreasing overall aspect ratio. Therefore, other factors must exceed the effect of aspect ratio, inducing a net red-shift. To understand the SPR features of the Au@Pt nanorods better, we investigated the effect of the L-ascorbic acid (AA) to Pt ratios on the formation of Pt nanostructures. Growth conditions with Pt nanodots grown at edges were employed. Figure 4 shows the UV/Vis/NIR absorption

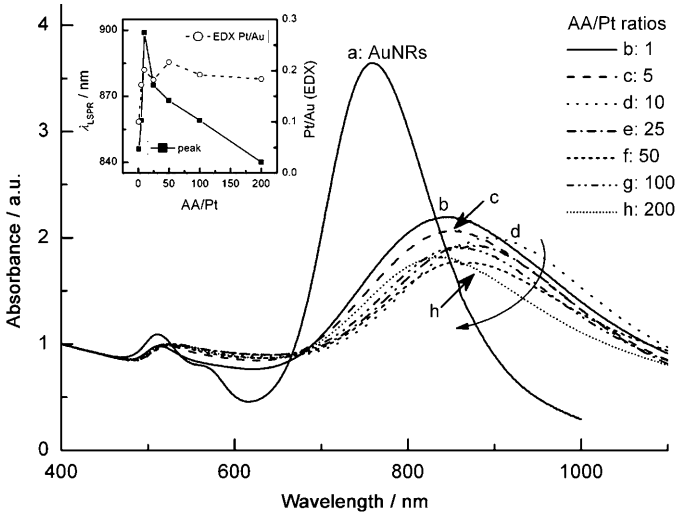

Figure 4. UV/Vis/NIR absorption spectra of a) the as-prepared Au NRs and b)–h) the Au@Pt NRs with AA/Pt molar ratios of 1, 5, 10, 25, 50, 100, and 200, respectively. The calculated Pt/Au molar ratio was kept at 0.17. Each spectrum was normalized by its absorption at 400 nm. Inset: Pt/Au molar ratio by EDX and peak position of LSPR band versus the AA/Pt ratio.

spectra of pure Au NRs and Pt-coated Au NRs with different AA/Pt ratios and with the Pt/Au ratio fixed at 0.17. The effect of the AA/Pt ratio on the Pt/Au ratio of the obtained Au@Pt nanorods (by EDX analysis) is exhibited in the inset of Figure 4. At AA/Pt ratios <10, the Pt/Au ratio in the Au@Pt nanorod increases with increasing AA/Pt ratio. At AA/Pt ratios >10, the obtained Pt/Au ratio reaches a plateau, indicating a complete conversion of the Pt ions to Pt atoms. The SEM images in Figure 5 support this conclusion. At AA/Pt ratios <10, the number of Pt nanodots is much smaller than those at AA/Pt ratios >10. For AA/Pt ratios of 10–200, the morphologies of the Pt shells are quite similar. Checking the LSPR bands, it is observed that both the decrease in intensity and the broadening in width indicate the damping due to the deposition of Pt. For the peak position of the LSPR band, an initial red-shift is seen at AA/Pt ratios <10 and then a blue-shift follows at AA/Pt ratios >10 (Figure 4 inset). Relative to the Au NRs, a maximum red-shift up to 135 nm has been achieved for the Au@Pt nanorods at the AA/Pt ratio of 10. By increasing AA/Pt ratios further, the LSPR is shifted back and a maximum blue-shift of 60 nm is reached at the AA/Pt ratio of 200 (in comparison with the AA/Pt ratio of 10). Commonly for metal nanorods, the shift of the LSPR band can be caused by changes in the aspect ratio, the surrounding dielectric constant, the composition, and the structure. The Au NRs have an LSPR band centered at 758 nm, corresponding to an aspect ratio of 3.55. The Au@Pt nanorods obtained at the

 © 2008 Wiley-VCH Verlag GmbH & Co. KGaA, Weinheim

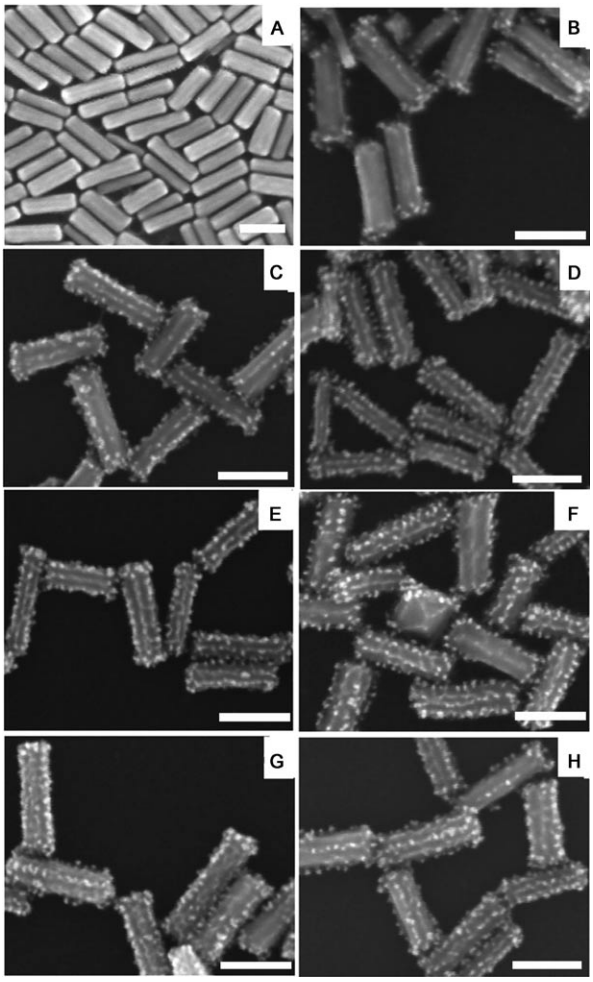

Figure 5. SEM images of A) the Au NRs and Au@Pt nanostructures obtained at AA/Pt ratios of B) 1, C) 5, D) 10, E) 25, F) 50, G) 100, and H) 200. The Pt/Au ratio was kept at 0.17. The scale bar is 50 nm.

AA/Pt ratio of 10 have an average length of 68 nm and an average width of 19 nm (average for 100 nanorods). The average aspect ratio is thus 3.58. There is no evident difference in the aspect ratio between the Au NRs and Au@Pt0. 17 NRs. Therefore, the large red-shift is not caused by the change in aspect ratio. Recently, it has been found that the SPR properties of noble metal nanoparticles are strongly related to their detailed structures. For instance, for a Pd nanocage with a wall thickness of 6 nm, its SPR band is centered at 520 nm.[7b] By decreasing the wall thickness to 3 nm, the SPR position can be pushed to 870 nm.[7b] Based on this, we believe that a very thin Pt layer shows an LSPR band at the near-infrared region. For the Au@Pt nanostructures, the SPR features can be considered as the combination of the Au core and Pt shell. Both the amount and the thickness of Pt determine its contribution to the final position and the strength of the overall SPR features. For a very thin Pt layer, on one hand, it has an SPR position at a longer wavelength; on the other hand, the low percentage of Pt in the core/shell structure leads to a small contribution and thus a small overall red-shift and less damping. With a further increase in the Pt thickness, although the SPR position of the Pt shell is blue-shifted a little (still at the longer wavelength compared to the Au core), its contribution to the core/shell nanorod increases, leading to more overall red-shift and stronger damping. A fine combination of Pt thickness and percentage gives rise to a maximum red-shift. This explanation can be extended to the red-shift of the LSPR maximum in Figure 2a–d. The blue-shift from the AA/Pt ratio of 10 to 200 can be explained by the tiny difference in the Pt thickness at the end and side. As shown in the inset of Figure 4, the obtained Pt/Au ratios are quite similar in these AA/Pt ratios and the SEM images also show no evident difference in morphology. However, due to the difference in growth rate, the thickness of the Pt layer at the end and at the side can be different. As is already known for the Au NR-seeded growth,[12,17] slow deposition favors the preferential deposition of metal at the two ends of the nanorod, thus inducing a greater thickness at the endcap compared with that at the side. In contrast, fast deposition deteriorates this preference and leads to more deposition at the side. In the case of Pt coating, the deposition rate can be tailored by the AA/Pt ratio. Increasing the AA/Pt ratio, more Pt is deposited at the side, thus inducing a greater side thickness and blue-shifting. Our results agree with the theoretical calculations by Grzelczak et al. They showed that the Pt thickness difference at the end and side of the Au NR can influence the LSPR position of Au@Pt nanorods.[12c] The 60 nm blue-shift therefore comes from variations in the detailed structure of the Pt shell obtained at different deposition parameters.

The increased dielectric sensitivity of Au@Pt nanorods: Due to the sharp and strong SPR features of Ag and Au nanostructures, one of their important applications is SPR-based sensing.[18,19] In contrast, for pure Pt nanostructures, owing either to an SPR band in the UV region (for spherical particles) or to quite a broad SPR band (for nonspherical particles), their potential in this aspect has not been exploited. However, Au@Pt nanorods with a thin Pt thickness have a well-defined LSPR band with a reasonable FWHM ($\approx$0.42 eV) in the visible and near-infrared region, thus making a study of their LSPR-based sensing possible. To investigate the dielectric sensitivity of Au@Pt nanorods, their absorption spectra were collected in water, dimenthyl sulfoxide (DMSO), and mixtures of water/DMSO in different volume ratios (Figure 6). The spectra show no evident changes in the width of the LSPR band, indicating that individual nanorods remain. As expected, the LSPR peak is red-shifted with the increase in the refractive index of the solvent. A good linear relationship is achieved with a slope of 441 nm RIU^{-1} (RIU = refractive index unit). For comparison, the results of the corresponding Au NR core are also demonstrated (Figure 7). Surprisingly, the Au@Pt nanorods had an even higher dielectric sensitivity than the Au core (361 nm RIU^{-1}).

To gain more insight into the increased dielectric sensitivity of the Au@Pt nanorods, we synthesized four Au NRs with different LSPR peak positions, and Au@Pt nanorods

 © 2008 Wiley-VCH Verlag GmbH & Co. KGaA, Weinheim

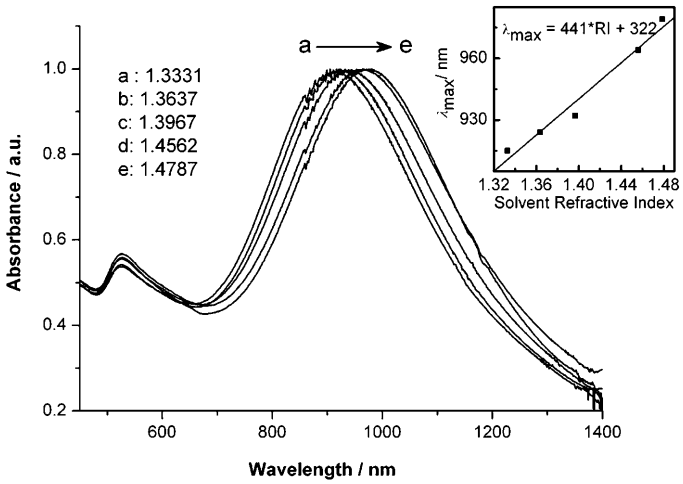

Figure 6. UV/Vis/NIR absorption spectra of the Au@Pt nanorods in the mixtures of water and DMSO with different volume ratios. The calculated Pt/Au molar ratio was kept at 0.17. Inset: Plot depicting the linear relationship between the solvent refractive index and the LSPR λ_{max}.

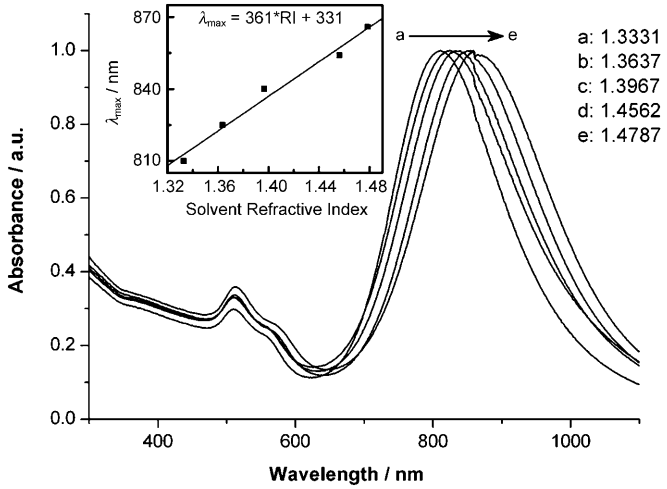

Figure 7. UV/Vis/NIR absorption spectra of Au NRs in the mixtures of water and DMSO with different volume ratios. Inset: Plot depicting the linear relationship between the solvent refractive index and the LSPR λ_{max}.

using the four Au NRs as seeds. As is already known, for the Au nanorods the dielectric sensitivity increases with increasing aspect ratio of the nanorod. The absorption spectra of Au NRs and Au@Pt nanorods are shown in Figure 8a. The number after the Au indicates the concentration of Ag^+ ions in the growth solution (see Experimental Section). Ag^+ ions are used to control the aspect ratio of the Au NRs. As illustrated in Figure 8a, with increasing Ag^+ concentration, the LSPR band of the Au NRs shifts to a longer wavelength due to an increase in aspect ratio. Upon deposition of a thin Pt shell, the LSPR bands of the Au@Pt nanorods are red-shifted compared with those of the Au cores. Although the LSPR band is damped and broadened a little, a well-defined band still exists. The dielectric sensitivities of the Au NRs

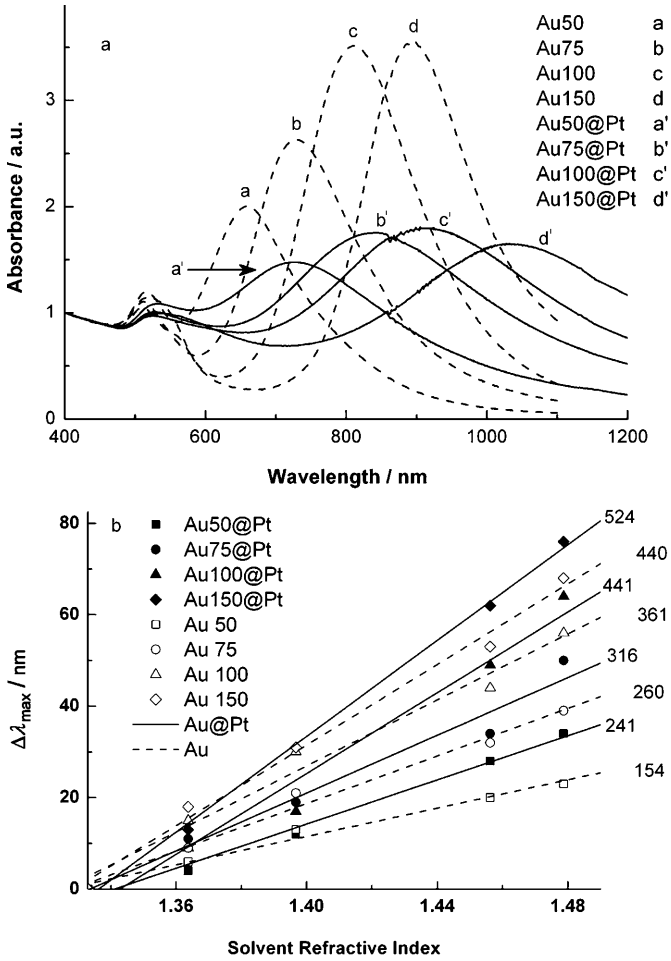

Figure 8. a) UV/Vis/NIR absorption spectra of the Au NRs with different aspect ratios and the corresponding Au@Pt nanorods. For the Au@Pt nanorods, the calculated Pt/Au molar ratio is kept at 0.17. b) Comparison of refractive index sensitivity for the Au NRs and the corresponding Au@Pt nanorods.

and Au@Pt nanorods are illustrated in Figure 8b. For the Au NRs, by pushing the LSPR maximum from 658 to 891 nm, the sensitivity increases from 154 to 440 nm RIU^{-1}. In the case of Au@Pt nanorods, by shifting the LSPR maximum from 727 to 1034 nm, the sensitivity increases from 241 to 524 nm RIU^{-1}. All Au@Pt nanorods show increased sensitivity compared to their corresponding Au cores, verifying their enhanced dielectric sensitivity. Raschke et al. investigated the dielectric sensitivity of Au_2S@Au core/shell nanoparticles and pure Au nanoparticles.[18c] It was found that Au_2S@Au nanoparticles have a higher dielectric sensitivity than Au nanoparticles of the same size. Interestingly, they also show a red-shifted SPR maximum compared with the Au nanoparticles. Similar observations have been obtained by other groups.[18a] We therefore believe that the enhanced sensitivity of the Au@Pt nanorods comes from the red-shifted LSPR band. A plot of the dielectric sensitivity versus the LSPR band maximum is shown in Figure 9. It is very interesting that the same straight line holds both for the Au NRs and for the Au@Pt nanorods. For the Au NRs, this linear re-

 © 2008 Wiley-VCH Verlag GmbH & Co. KGaA, Weinheim

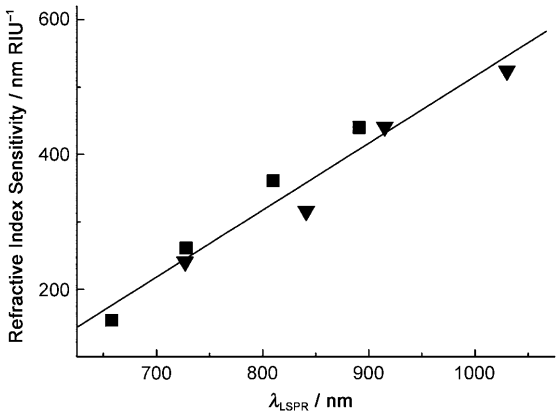

Figure 9. The relationship of the refractive index sensitivity of the Au NRs and the Au@Pt nanorods with the peak position of the LSPR bands. The data points from the Au NRs and the Au@Pt nanorods are represented by squares and triangles, respectively. The straight line is a linear regression to all data points.

lationship has been verified. For the Au@Pt nanorods, we guess, due to the very thin Pt layer, the LSPR properties are still dominated by the Au core. Thus, the linear relationship for pure Au NRs can be extended to Au@Pt nanorods.

Conclusion

We have presented a simple wet-chemical method to tailor finely the growth of Pt nanodots on the Au nanorod. Both edge-growth and homogeneous coating can be achieved. By forming a core/shell structure with the Au NR, the LSPR band of the Pt nanostructures can be easily pushed to the visible and near-infrared region. At thin Pt thickness, the Au@Pt nanorods show a well-defined and red-shifted LSPR band in comparison with the Au cores. Beneficial from the red-shift, they exhibit a higher dielectric sensitivity than the corresponding Au NRs. Thus the potential of Pt nanostructures for SPR-based sensing are opened up.

Experimental Section

Sodium borohydride ($NaBH_4$; AR, purity $>98.0\%$), chlorauric acid ($HAuCl_4{\cdot}3H_2O$; AR, Au content $\geq 47.8\%$), cetyltrimethylammonium bromide (CTAB; AR, purity $>99.0\%$), poly(sodium-p-styrensulfonate) (PSS, Mw 70000; AR), silver nitrate ($AgNO_3$; AR) and L-ascorbic acid (AA; AR, purity $>99.0\%$), and potassium tetrachloroplatinate(II) (K_2PtCl_4; AR, Pt content $\geq 46.0\%$) were obtained from Alfa and used as received without further purification. Milli-Q water (18 MΩ cm) was used for all solution preparations. All glassware used in the following procedures was cleaned in a bath of a piranha solution (H_2SO_4/30 % H_2O_2 = 7:3 v/v) and boiled for 30 min.

Synthesis of the Au NRs: Au NRs were synthesized by using a seed-mediated growth procedure. CTAB-capped Au seeds were synthesized by chemical reduction of $HAuCl_4$ with $NaBH_4$: CTAB (7.5 mL, 0.1 M) was mixed with $HAuCl_4$ (100 μL, 24 mM), diluted with water to 9.4 mL, and stirred with a magnetic stirrer. Then, ice-cold $NaBH_4$ (0.6 mL, 0.01 M) was added. The solution color immediately turned from bright yellow to brown, indicating the formation of good seeds. The Au seeds were used within 2–5 h. The growth solution for the formation of the Au nanorods consisted of CTAB (100 mL, 0.1 M), $HAuCl_4$ (2.04 mL, 0.024 M), H_2SO_4 (2 mL, 0.5 M), $AgNO_3$ (1 mL, 10 mM), and AA (800 μL, 0.1 M). Then the seed solution (240 μL) was added to the above growth solution to initiate the growth of the Au NRs. After 12 h, the reaction was stopped. The obtained Au nanorods were purified by centrifuging the solution at 12000 rpm for 5 min twice. The precipitates were collected and redispersed in deionized water, and the volume changed to half that of the original solution.

Synthesis of Au@Pt nanostructures with different Pt/Au ratios: Six samples of the purified Au NR solutions (1 mL) were each mixed with a different volume (46.8, 79.6, 117, 234, 550, or 937 μL) of 2 mM $PtCl_4^{2-}$ [K_2PtCl_4 (0.0688 g) was dissolved in aqueous HCl solution (2 mL, 0.2 M) and then diluted to 100 mL with deionized water]. The corresponding Pt/Au ratios are 0.1, 0.17, 0.25, 0.5, 1.17, and 2, respectively. Then, different amounts of AA (keeping AA/$PtCl_4^{2-}$ molar ratio = 10) were added and the total solution volume was diluted to 3 mL. The mixtures were then shaken vigorously and placed in a water bath at 30 °C. Within several minutes, the color of the solution changed from pink-red to dark gray, suggesting the formation of a Pt shell. After being undisturbed for 14 h in the water bath, the Au@Pt nanostructures were separated from the growth solution by centrifugation (12000 rpm, 10 min). The precipitates were redispersed in deionized water.

Synthesis of Au NRs with different aspect ratios and Au@Pt nanorods with different Au cores: The aspect ratio of the Au NRs can be tuned simply by changing the concentration of silver ions in the growth solution. Therefore, we distinguish the different Au NRs using the concentrations of silver ions. For example, in the above case, the concentration of silver ions in the growth solution is ≈100 μM; we therefore named the obtained Au NRs as Au100. Similarly, for silver concentrations of 50, 75, and 150 μM, the corresponding Au NRs are named as Au50, Au75, and Au150, respectively. For the formation of Au@Pt nanorods on different Au cores, the growth conditions for Au@Pt nanorods with the Pt/Au ratio of 0.17 were employed.

Modification of the Au NRs and the Au@Pt nanorods with PSS: To investigate the dielectric sensitivity of the LSPR band, mixtures of water and DMSO in different volume ratios were used to fabricate solvents with different refractive indices. The refractive indices of water, DMSO, and water/DMSO mixtures were measured with an Abbe refractormeter. Due to the aggregation of CTAB-capped Au NRs in the mixtures of water and DMSO, PSS-modified Au NRs were employed for dielectric sensitivity measurements. The preparation of PSS-modified Au NRs is as follows: CTAB-coated nanorod solution (12 mL, either Au NRs or Au@Pt nanorods) was centrifuged at 12000 rpm for 10 min, and the precipitate was dispersed in PSS aqueous solution (2 mg mL^{-1}, 12 mL, containing 6 mM NaCl). Then the solution was stirred magnetically for 3 h. After that, it was centrifuged at 12000 rpm for 10 min, and the precipitate was redispersed in water, dimethyl sulfoxide (DMSO), or a mixture of water/DMSO with different volume ratio.

UV/Vis/NIR absorption spectra were recorded using a Perkin–Elmer Lamdba 950. For transmission electron microscopy (TEM, Tecnai F30) and scanning electron microscopy (SEM, Hitachi S-5200) measurements, centrifugations (12000 rpm 10 min) were applied twice.

Acknowledgements

This work was supported by the National Natural Science Foundation of China (Grant No. 20773032) and the "973" National Key Basic Research Program of China (2006CB705600 and 2006CB932602).

[1] a) R. Narayanan, M. A. El-Sayed, *Nano Lett.* **2004**, *4*, 1343; b) Y. Li, J. Petroski, M. A. El-Sayed, *J. Phys. Chem. B* **2000**, *104*, 10956; c) R. Narayanan, M. A. El-Sayed, *J. Am. Chem. Soc.* **2004**, *126*, 7194; d) J. Y. Chen, B. Wiley, J. McLellan, Y. J. Xiong, Z. Y. Li, Y. N. Xia,

 © 2008 Wiley-VCH Verlag GmbH & Co. KGaA, Weinheim

Nano Lett. **2005**, *5*, 2058; e) N. Tian, Z. Y. Zhou, S. G. Sun, Y. Ding, Z. L. Wang, *Science* **2007**, *316*, 732.

[2] a) H. Song, F. Kim, S. Connor, G. A. Somorjai, P. D. Yang, *J. Phys. Chem. B* **2005**, *109*, 188; b) H. Lee, S. E. Habas, S. Kweskin, D. Butcher, G. A. Somorjai, P. D. Yang, *Angew. Chem.* **2006**, *118*, 7988; *Angew. Chem. Int. Ed.* **2006**, *45*, 7824; c) J. Y. Chen, T. Herricks, Y. N. Xia, *Angew. Chem.* **2005**, *117*, 2645; *Angew. Chem. Int. Ed.* **2005**, *44*, 2589; d) T. Herricks, J. Y. Chen, Y. N. Xia, *Nano Lett.* **2004**, *4*, 2367; e) X. W. Teng, H. Yang, *Nano Lett.* **2005**, *5*, 885.

[3] a) Y. J. Song, Y. Yang, C. J. Medforth, E. Perer, F. van Swol, J. A. Shelnutt, *J. Am. Chem. Soc.* **2004**, *126*, 635; b) X. W. Teng, X. Y. Liang, S. Maksimuk, H. Yang, *Small* **2006**, *2*, 249; c) H. P. Liang, H. M. Zhang, J. S. Hu, Y. G. Guo, L. J. Wan, C. L. Bai, *Angew. Chem.* **2004**, *116*, 1566; *Angew. Chem. Int. Ed.* **2004**, *43*, 1540.

[4] H. G. Lang, S. Maldonado, K. J. Stevenson, B. D. Chandler, *J. Am. Chem. Soc.* **2004**, *126*, 12949.

[5] S. G. Zhou, K. McIlwrath, G. Jackson, B. Eichhorn, *J. Am. Chem. Soc.* **2006**, *128*, 1780.

[6] D. Zhao, B. Q. Xu, *Angew. Chem.* **2006**, *118*, 5077; *Angew. Chem. Int. Ed.* **2006**, *45*, 4955.

[7] a) Y. J. Xiong, J. M. Mclellan, J. Y. Chen, Y. D. Yin, Z. Y. Li, Y. N. Xia, *J. Am. Chem. Soc.* **2005**, *127*, 17118; b) Y. J. Xiong, B. Wiley, J. Y. Chen, Z. Y. Li, Y. D. Yin, Y. N. Xia, *Angew. Chem.* **2005**, *117*, 8127; *Angew. Chem. Int. Ed.* **2005**, *44*, 7913.

[8] a) L. H. Lu, G. Y. Sun, H. J. Zhang, H. S. Wang, S. Q. Xi, J. Q. Hu, Z. Q. Tian, R. Chen, *J. Mater. Chem.* **2004**, *14*, 1005; b) B. Zhang, J. F. Li, Q. L. Zhong, B. Ren, Z. Q. Tian, S. Z. Zou, *Langmuir* **2005**, *21*, 7449.

[9] a) A. Henglein, *J. Phys. Chem. B* **2000**, *104*, 2201; b) L. Y. Cao, L. M. Tong, P. Diao, T. Zhu, Z. F. Liu, *Chem. Mater.* **2004**, *16*, 3239.

[10] L. Qian, X. R. Yang, *J. Phys. Chem. B* **2006**, *110*, 16672.

[11] a) N. R. Jana, L. Gearheart, C. J. Murphy, *Adv. Mater.* **2001**, *13*, 1389; b) B. Nikoobakht, M. A. El-Sayed, *Chem. Mater.* **2003**, *15*, 1957; c) L. F. Gou, C. J. Murphy, *Chem. Mater.* **2005**, *17*, 3668.

[12] a) M. B. Mohamed, V. Volkov, S. Link, M. A. El-Sayed, *Chem. Phys. Lett.* **2000**, *317*, 517; b) K. Imura, T. Nagahara, H. Okamoto, *J. Phys. Chem. B* **2005**, *109*, 13214; c) J. F. Li, Z. L. Yang, B. Ren, G. K. Liu, P. P. Fang, Y. X. Jiang, D. Y. Wu, Z. Q. Tian, *Langmuir* **2006**, *22*, 10372.

[13] a) M. Grzelczak, J. Perez-Juste, B. Rodriguez-Gonzalez, L. M. Liz-Marzan, *J. Mater. Chem.* **2006**, *16*, 3946; b) S. Guo, L. Wang, Y. Wang, Y. Fang, E. Wang, *J. Colloid Interface Sci.* **2007**, *315*, 363; c) M. Grzelczak, J. Perez-Juste, F. J. G. De Abajo, L. M. Liz-Marzan, *J. Phys. Chem. C* **2007**, 111, 6183.

[14] J. H. Song, F. Kim, D. Kim, P. D. Yang, *Chem. Eur. J.* **2005**, *11*, 910.

[15] a) J. D. Hoefelmeyer, K. Niesz, G. A. Somorjai, T. D. Tilley, *Nano Lett.* **2005**, *5*, 435; b) Y. J. Song, Y. B. Jiang, H. R. Wang, D. A. Pena, Y. Qiu, J. E. Miller, J. A. Shelnutt, *Nanotechnology* **2006**, *17*, 1300.

[16] Y. J. Xiang, X. C. Wu, D. F. Liu, X. Y. Jiang, W. G. Chu, Z. Y. Li, Y. Ma, W. Y. Zhou, S. S. Xie, *Nano Lett.* **2006**, *6*, 2290.

[17] a) C. C. Huang, Z. Yang, H. T. Chang, *Langmuir* **2004**, *20*, 6089; b) Z. Yang, H. T. Chang, *Nanotechnology* **2006**, *17*, 2304.

[18] a) A. D. McFarland, R. P. Van Duyne, *Nano Lett.* **2003**, *3*, 1057; b) J. J. Mock, D. R. Smith, S. Schultz, *Nano Lett.* **2003**, *3*, 485; c) G. Raschke, S. Brogl, A. S. Susha, A. L. Rogach, T. A. Klar, J. Feldmann, B. Fieres, N. Petkov, T. Bein, A. Nichtl, K. Kuezinger, *Nano Lett.* **2004**, *4*, 1853; d) J. Yang, J. C. Wu, Y. C. Wu, J. K. Wang, C. C. Chen, *Chem. Phys. Lett.* **2005**, *416*, 215.

[19] K. Lee, M. A. El-Sayed, *J. Phys. Chem. B* **2006**, *110*, 19220.

Received: March 25, 2008
Revised: July 4, 2008
Published online: September 4, 2008

 © 2008 Wiley-VCH Verlag GmbH & Co. KGaA, Weinheim